PNAS NEXUS

PNAS Nexus, 2025, **4**, pgae544

https://doi.org/10.1093/pnasnexus/pgae544
Advance access publication 28 November 2024
Research Report

Modulation of microtubule dynamics by monovalent ions

Simon Fernandes[a] and Charlotte Aumeier[a,*]

[a]Department of Biochemistry, University of Geneva, 1211 Geneva, Switzerland
*To whom correspondence should be addressed: Email: charlotte.aumeier@unige.ch
Edited By Gerhard Hummer

Abstract

The microtubule cytoskeleton is a dynamic network essential for many cellular processes, influenced by physicochemical factor, such as temperature, pH, dimer concentration, and ionic environment. In this study, we used in vitro reconstitution assays to examine the effects of four monovalent ions (Na^+, K^+, Cl^-, and Ac^-) on microtubule dynamics, uncovering distinct effects for each ion. Na^+ was found to increase microtubule dynamicity by raising catastrophe frequency, polymerization and depolymerization speeds, and ultimately reducing microtubule lifetime by 80%. Conversely, Ac^- boosts microtubule nucleation and stabilizes microtubules by increasing rescue frequency and preventing breakages, resulting in longer microtubules with extended lifetimes. Cl^- appeared to potentiate the effects of Na^+, while K^+ had minimal impact on microtubule dynamic parameters. These findings demonstrate that Na^+ and Ac^- have opposing effects on microtubule dynamics, with Na^+ destabilizing and Ac^- stabilizing the microtubule structure. This ionic impact is mainly through modulation of tubulin–tubulin interactions rather than affecting the hydrolysis rate. In conclusion, ion identity plays a crucial role in modulating microtubule dynamics. Understanding the ionic environment is essential for microtubule-related research, as it significantly influences microtubule behavior, stability, and interactions with other proteins.

Keywords: microtubule dynamics, microtubule nucleation, microtubule damage, monovalent ions

Significance Statement

The microtubule cytoskeleton is vital for cellular processes, and its behavior is influenced by factors, such as temperature, pH, concentration of building blocks, and ionic environment. Understanding how these factors regulate microtubule dynamics and stability gives insight into their function in cells. Our in vitro reconstitution assays reveal that sodium (Na^+) and acetate (Ac^-) ions have opposite effects on microtubule dynamics. Na^+ makes microtubules more dynamic by inducing depolymerization and thereby shortening their lifetime by 80%, while Ac^- supports microtubule formation and stability, resulting in longer microtubules. Additionally, chloride (Cl^-) enhances Na^+'s destabilizing effects, whereas potassium ion (K^+) has little influence. Our findings highlight that ion identity crucially modulates microtubule formation, dynamics, and stability.

Introduction

The microtubule cytoskeleton is a highly dynamic network, conserved throughout all eukaryotes. Composed of αβ-tubulin heterodimers, microtubules are polarized hollow tubes that form by longitudinal and lateral interactions between the dimers (1, 2). Temperature, pH, and dimer concentration are central factors to determine the fate of the biopolymer (1, 3, 4). Moreover, pioneer studies using reconstituted in vitro assays demonstrated that the ionic composition is a major player in microtubule biochemistry, impacting microtubule dynamics (5–10).

Microtubules polymerize by the addition of guanosine-5′-triphosphate (GTP)-tubulin dimers at their ends (11). After incorporation, GTP is hydrolyzed to guanosine diphosphate (GDP), resulting in an unstable GDP microtubule in comparison with the growing GTP-microtubule end that is stabilizing the structure (12, 13). Over time the structure of the growing end becomes more irregular, tapered, reducing the local concentration of GTP tubulin. When GTP hydrolysis is faster than the addition of new GTP-tubulin dimers, colliding with a reduction of the local GTP-tubulin density, the unstable microtubule undergoes catastrophe followed by rapid depolymerization (14–16). Moreover, shrinking microtubules can switch back to regrowth, an event called rescue (16). Neither the addition or the dissociation of tubulin is restricted to microtubule ends; they can happen spontaneously all along the shaft (17–21). Indeed, damages along the shaft can be repaired by the incorporation of fresh GTP-tubulin dimers which can act as rescue sites (22). Altogether, these dynamic parameters, polymerization and depolymerization rates, along with rescue and catastrophe frequencies, govern the microtubule lifetime.

Ions finetune protein-to-protein interaction by changing the strength of electrostatic interactions (23, 24). In this scenario, tubulin–tubulin interactions during polymerization are subjected

Competing Interest: The authors declare no competing interests.
Received: June 27, 2024. **Accepted:** November 20, 2024

to this electrostatic modulation. Once formed, microtubules exhibit electronegative charges at their surfaces that can be mitigated by the presence of ions, which, in turn, can alter interactions with microtubule-associated proteins (25, 26). Moreover, ions exhibit different lyotropic properties, impacting the solubilization of proteins and, therefore, protein stability in solution (27–30). This ability of ions to stabilize or destabilize proteins in solution could be relevant in the context of microtubule polymerization as soluble tubulin heterodimers polymerize into an insoluble microtubule.

Early studies on microtubule polymerization addressed the role of ions in microtubule assembly. The divalent cations Magnesium (Mg^{2+}) and Calcium (Ca^{2+}) were rapidly identified to influence microtubule dynamics (6, 31). Mg^{2+} binds to the tubulin GTP pocket and acts as a co-factor for GTP hydrolysis. Consequently, microtubule growth is impaired when Mg^{2+} is chelated by ethylenediaminetetraacetic acid during the polymerization reaction (32–36). However, concentrations of Mg^{2+} above 10 mM destabilize microtubules, probably by modulating the electrostatic interactions between tubulins. Ca^{2+} destabilizes microtubule integrity even more efficiently by increasing the catastrophe frequency and the depolymerization rate (31, 36–38). Concentrations under 1 mM Ca^{2+} already impair microtubule growth, and the addition of ethylene glycol tetraacetic acid (EGTA) rescues microtubule formation by chelating Ca^{2+} (6). Those findings set the base for the in vitro microtubule research.

Monovalent ions also impact microtubule dynamics, although in comparison with divalent cations, higher concentrations are needed to achieve effects. Concentrations of monovalent salts above 250 mM prevented microtubule formation and induced tubulin aggregation (4), while at physiological concentration (50–150 mM), ions such as alkali monovalent cations favored microtubule formation in the presence of Taxol, a microtubule-stabilizing drug (9, 39). In particular, sodium (Na^+) or potassium (K^+) showed an enhancement of the net microtubule formation (39). Similarly, monovalent anions, including acetate (Ac^-), glutamate, and fluoride, enhanced the net microtubule mass (9). However, all these experiments were performed in bulk experiments and a comprehensive investigation into the role of monovalent ions on direct dynamical features of microtubules is missing.

Here, we show how four different monovalent ions—Na^+, K^+, Cl^-, and Ac^-—affect microtubule dynamics and stability. Na^+ increases microtubule dynamicity by raising catastrophe frequency and enhancing polymerization and depolymerization speeds at the microtubule ends. In contrast, Ac^- promotes microtubule nucleation and extends microtubule length and lifetime by enhancing rescue frequency and reducing depolymerization frequency. Additionally, the effects of these salts on microtubule stability are independent of GTP hydrolysis, as they similarly influence microtubules in both GDP-tubulin and GTP-tubulin states. Our study shed light on the complex interplay of ions in microtubule assembly, providing insights into the mechanistic aspects of tubulin polymerization and microtubule biochemistry.

Results

Effect of ions on microtubule bulk dynamics

We selected KCl, NaCl, KAc, and NaAc as salts to distinguish how individual monovalent ions, Na^+, K^+, Cl^-, and Ac^-, as well as associative cation–anion effects impact on microtubule dynamics. Microtubules were polymerized from 15 μM tubulin using the BRB buffer in the absence or presence of the different ions at concentrations of 50 or 100 mM. Initially, we studied the influence of these salts on net microtubule mass formation using a turbidity assay (Fig. 1a). In the presence of 100 mM KAc, we saw the fastest microtubule nucleation (smallest lag time, 352 s), the fastest bulk polymerization (steepest slope, 2.07×10^{-4} a.u./s) reaching the highest polymer mass (plateau at 0.1171 a.u.; Fig. 1b). Microtubules grown in the presence of 100 mM NaAc had comparable bulk dynamics. The addition of KCl showed a turbidity profile comparable with the control condition (Fig. 1a and b). The presence of NaCl marginally decreased net microtubule formation, resulting in the lowest plateau values compared with the control. Therefore, KAc and NaAc are potent enhancers of microtubule formation, whereas NaCl might have a destabilizing effect.

To validate those observations with a complementary bulk assay, we performed a pelleting assay wherein microtubules were polymerized from 10 μM tubulin for 30 min in the presence or absence of 200 mM salt. Doubling the salt concentration aimed to intensify the measured salt effects in Fig. 1a. In the presence of 200 mM KAc, the polymerized fraction in the pellet increased by 2.5-fold compared with the control, confirming its stabilizing effect on net microtubule formation (Fig. 1c and d). Microtubule formation in the presence of 200 mM NaCl was comparable with control (Fig. 1d).

Effect of ions on single microtubule dynamics

While a bulk assay offers valuable insights, it lacks the resolution to discern whether higher polymer mass results from enhanced nucleation, polymerization, or stabilizing effects. To delve deeper into understanding the impact of the different salts on the parameters of microtubule dynamics—such as growth speed, depolymerization speed, catastrophe, and rescue frequency—we studied the dynamic parameters of single microtubules polymerized from seeds using a total internal reflection fluorescence (TIRF) microscopy-based assay (Fig. 2). We used 0 to 100 mM salt concentrations, as at higher concentrations, the analysis of microtubule dynamics was not possible for NaCl and KAc (Fig. 2a).

In our control condition (0 mM salt, in BRB80), 7 μM tubulin polymerized into microtubules at a speed of 0.36 ± 0.01 μm/min (Fig. 2c). Contrary to expectations from the bulk assay, microtubule growth speed increased only slightly with the addition of 50 or 100 mM KAc (Fig. 2c). During growth, the polymerization speed of individual microtubules fluctuated in the presence of KAc, with periods where growth even appeared to pause (Figs. 2b and S1a). Adding 100 mM KCl to the assay reduced the polymerization speed to 0.21 ± 0.07 μm/min (Fig. 2c). Conversely, the addition of either 50 mM NaCl or NaAc doubled the growth speed compared with the control (Table 1). Doubling the salt concentration to 100 mM only marginally further increased growth speed to 2.2-fold. However, at a concentration of 150 mM, both salts had contrasting effects: 150 mM NaCl completely inhibited polymerization, while 150 mM NaAc led to highly dynamic microtubules and spontaneous nucleation (Fig. 2a). Collectively, these results show that salts containing the cation Na^+ increase microtubule growth speed and indicate that the anion partners do not differentially affect the growth up to 100 mM but have a differential impact at higher concentrations (Fig. S1b).

We next studied how the different salts impact microtubule catastrophe events. Both KAc and KCl had no significant impact on catastrophe events (Fig. 2d). In contrast, the catastrophe frequency increased up to 5-fold in the presence of salts containing Na^+, with NaCl amplifying the frequency nearly twice as much as NaAc (Fig. 2d). Combining 25 mM NaCl with 25 mM NaAc (50 mM Na^+ in total) yielded comparable results to conditions

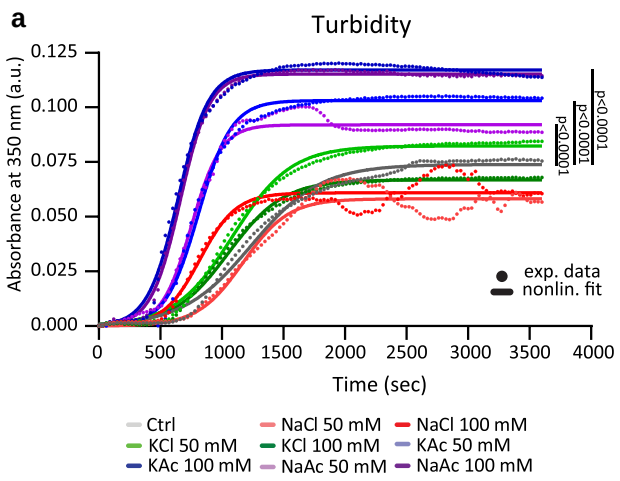

b

Salt	Lag time (sec)	Plateau (Abs_{350})	Slope(a.u./sec)
Control	664	0.0738	6.81E-05
KCl 50 mM	576	0.0823	8.64E-05
KCl 100 mM	580	0.0668	6.77E-05
NaCl 50 mM	643	0.0581	5.69E-05
NaCl 100 mM	530	0.0609	8.54E-05
KAc 50 mM	464	0.1031	1.44E-04
KAc 100 mM	352	0.1171	2.07E-04
NaAc 50 mM	469	0.0920	1.21E-04
NaAc100 mM	372	0.1152	1.91E-04

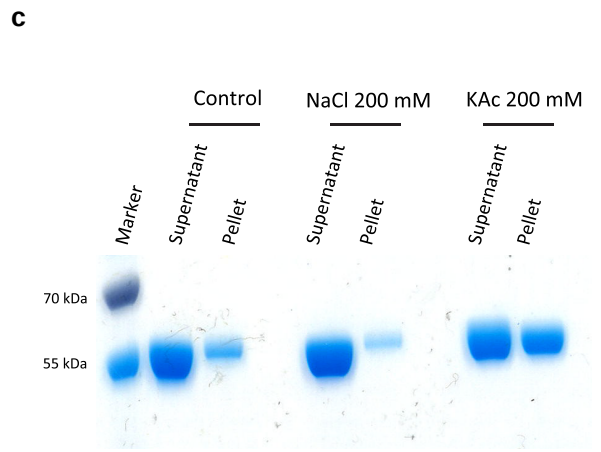

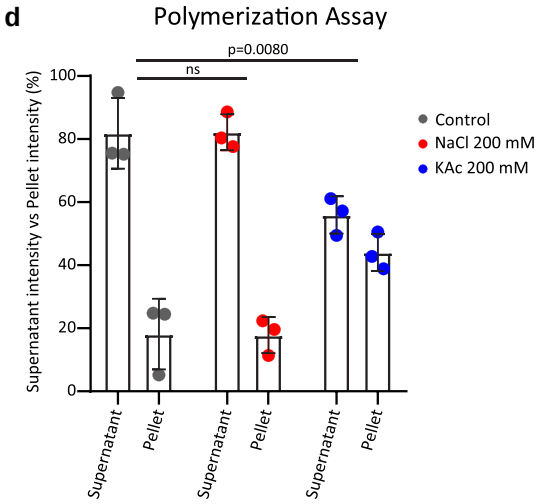

Fig. 1. Ion effect on bulk polymerization. a) Representative turbidity assay of 15 μM tubulin in the presence of the indicated salts. Absorbance at 350 nm was recorded every 30 s at 37 °C. Experimental data are represented by colored dots. A nonlinear fit (logistic growth) for each condition is plotted as a colored solid line. Statistics: one-way ANOVA. b) Lag time, plateau, and slope were calculated from the nonlinear fit of the turbidity assay (panel a; see Materials and methods). c) Pelleting assay of 10 μM tubulin. Microtubules were polymerized for 30 min at 37 °C in BRB80 with 1 mM GTP, 20% (v/v) glycerol, and 200 mM of the indicated salt. Representative SDS–PAGE with supernatant and pellets after 30 min polymerization at 37 °C. d) Quantification of band intensity of (c). Mean with SD, $n = 3$ independent experiments. Statistics: two-way ANOVA.

with 50 mM NaCl alone (Fig. S1c), indicating that the increase in catastrophe events is caused by the Na^+ cation. This is further supported by the results from a combination of 50 mM KAc and 50 mM NaAc (50 mM Na^+ in total), showing a frequency comparable with that in the presence of 50 mM NaAc.

Upon catastrophe, the depolymerization speed was not altered in the presence of KAc, KCl, nor NaAc, while 50 mM NaCl nearly doubled the depolymerization speed compared with control (Fig. 2e and Table 1). This result indicates that increasing depolymerization velocities may depend on the cooperative effect between Na^+ and Cl^-. Doubling the NaCl concentration to 100 mM did not further increase the depolymerization speed. Microtubule depolymerization can occur in distinct phases with distinct speeds, though the net depolymerization speed remains constant (40). To test whether salts induce different depolymerization phases, we imaged at 1 s per frame. No alteration in depolymerization slopes was observed, indicating that depolymerization under the different conditions happened in a single regime (Fig. S1f and g).

Rescue events were rare, with a frequency of $0.95 \pm 0.26\ min^{-1}$ in control conditions and remained rare in the presence of KCl or NaCl (Fig. 2f). However, the rescue frequency increased up to 5-fold in the presence of Ac^- containing salts, reaching $5.11 \pm 0.21\ min^{-1}$ for the highest concentration of 100 mM NaAc. The rescue-induced effect was observed even with a combination of 25 mM NaCl and 25 mM NaAc (total 25 mM Ac^-), which tripled the rescue frequency compared with the control (Fig. S1e). Collectively, salts with the anion Ac^- boosted the rescue frequency, while those with the Cl^- anion did not significantly affect rescue (Fig. 2f).

Taken together, 50 mM KCl did not have a discernible impact on any of the microtubule dynamic parameters, explaining its preference in in vitro microtubule assays for modulating buffer ionic strength. The two main ions controlling dynamics are Na^+ and Ac^-. While the cation Na^+ boosts polymerization speed, it simultaneously is the major destabilizing factor by increasing the catastrophe frequency and the depolymerization speed, thereby increasing the dynamicity of microtubules. The presence of Cl^- might further potentiate Na^+ effects. Conversely, the presence of Ac^- increases the rescue frequency.

Acetate increases microtubule mass

Microtubules that undergo rescue are longer due to an extended net growth phase (41, 42). Consistently, we measured a 2-fold increase in the mean microtubule length in the presence of 100 mM KAc compared with the control (Figs. 2b and 3a). The mean length

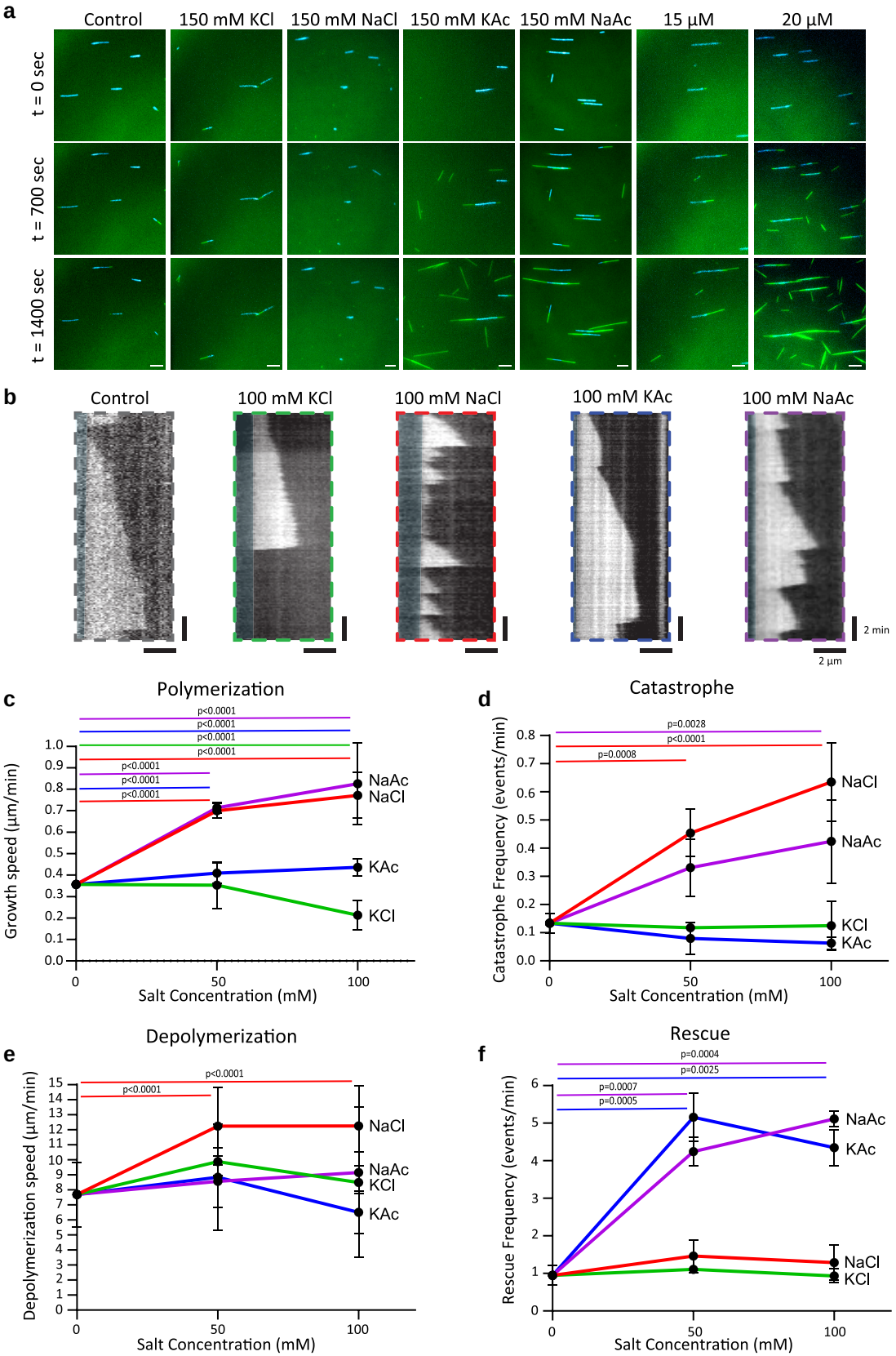

Fig. 2. Ion effect on single microtubule dynamics. a) Representative images at three different time points (0, 700, and 1,400 s) of dynamic microtubule at 7 µM tubulin with 0 or 150 mM indicated salt. GMPCPP-stabilized microtubules (seeds) are in cyan, dynamic microtubules are in green. Scale bar: 5 µm. b) Representative kymographs of microtubules (7 µM tubulin). Control (0 mM salt, gray), 100 mM KCl (green), 100 mM NaCl (red), 100 mM KAc (blue), and 100 mM NaAc (purple). c–f) Mean microtubule growth speed (c), mean microtubule catastrophe frequency (d), mean microtubule depolymerization speed (e), and mean microtubule rescue frequency (f) (7 µM tubulin) with 0, 50, or 100 mM indicated salts. Experimental mean with SD, $n = 3$ independent experiments. Statistics: one-way ANOVA (the colored code was kept for statistics), the full statistic comparison between all conditions, individual and experimental mean values in Fig. S1a–d.

Table 1. Microtubule dynamics according to the ionic composition of the buffer.

Salt	Growth speed (µm/min)	Shrikage speed (µm/min)	Catastrophe frequency (events/min)	Rescue frequency (events/min)
Control	0.36 ± 0.01	7.69 ± 2.15	0.13 ± 0.03	0.95 ± 0.26
50 mM KCl	0.35 ± 0.01	9.87 ± 0.94	0.12 ± 0.01	1.11 ± 0.09
100 mM KCl	0.21 ± 0.07	8.49 ± 5.01	0.12 ± 0.09	0.93 ± 0.18
50 mM NaCl	0.69 ± 0.03	12.24 ± 2.58	0.45 ± 0.08	1.46 ± 0.45
100 mM NaCl	0.77 ± 0.11	12.25 ± 2.68	0.64 ± 0.14	1.29 ± 0.47
50 mM KAc	0.40 ± 0.05	8.82 ± 3.55	0.08 ± 0.06	5.16 ± 0.65
100 mM KAc	0.43 ± 0.03	6.51 ± 1.43	0.06 ± 0.02	4.35 ± 0.48
50 mM NaAc	0.71 ± 0.02	8.57 ± 1.40	0.33 ± 0.10	4.24 ± 0.38
100 mM NaAc	0.82 ± 0.19	9.15 ± 1.38	0.42 ± 0.15	5.11 ± 0.21

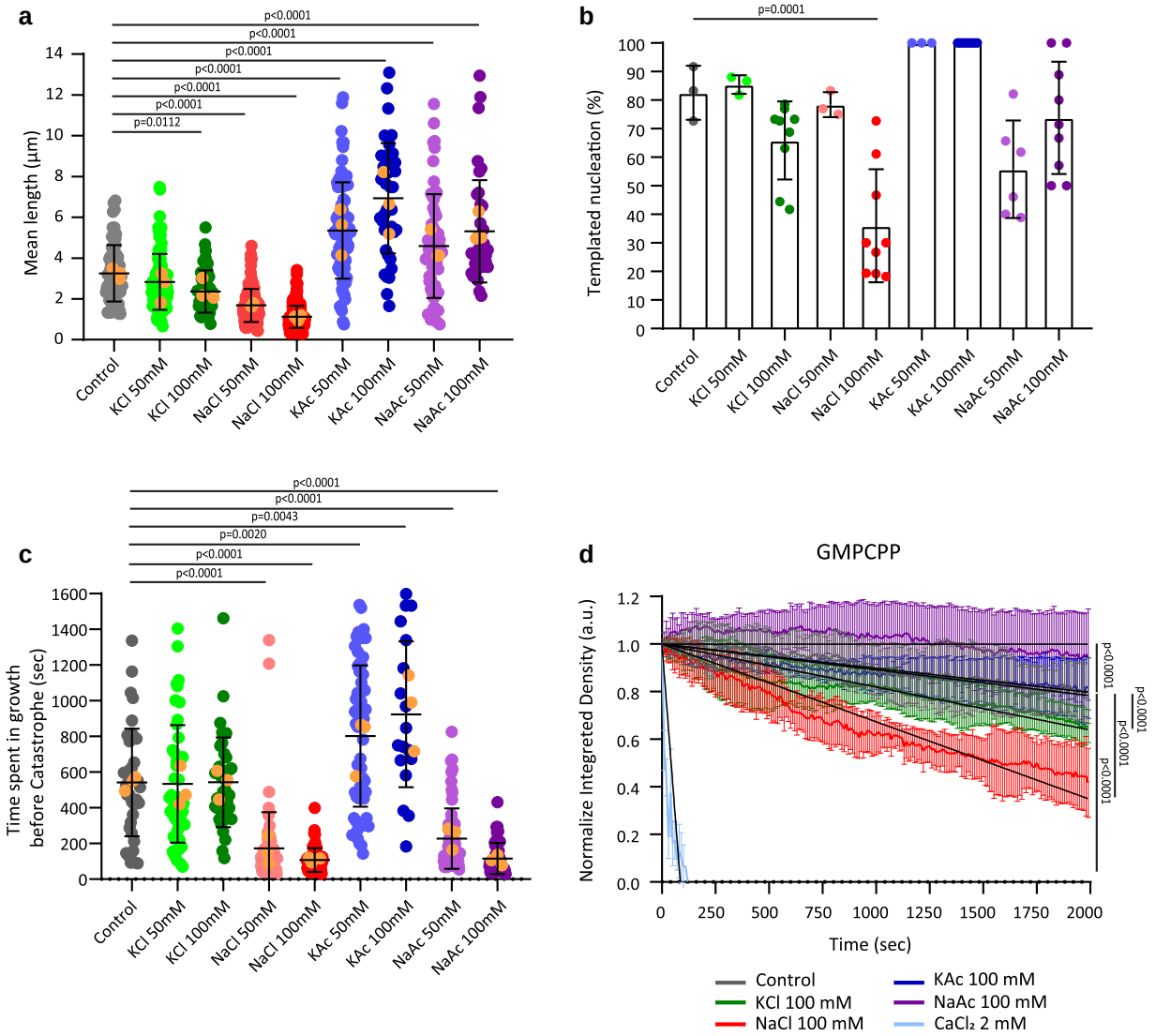

Fig. 3. Ion effect on microtubule stability and nucleation. a) Mean microtubule length (7 µM tubulin) over 45 min with the indicated salt. The length was calculated from the cumulative length of single microtubules. Mean with SD, $n = 3$ independent experiments, individual values, and experimental means (orange dots). b) Mean ratio of templated microtubule nucleation within 45 min (number of seeds with microtubule/total number of seeds in the field of view): 7 µM tubulin, with the indicated salt. Experimental mean with SD, $n = 3$ to 10 independent experiments. c) Mean microtubule lifetime until the first catastrophe event (7 µM tubulin) with the indicated salt. Mean with SD, $n = 3$ independent experiments, individual values, and experimental means (orange dots). d) Normalized mean integrated fluorescent density of GMPCPP microtubules (survival assay, see Materials and methods) was measured every 10 s over 200 frames. Experimental data are in colored lines, and the linear regressions are in black (see Materials and methods). Mean with SD, $n = 3$ independent experiments. a–d) Statistics: one-way ANOVA, for clarity only significant values are shown in the graph.

of microtubules grown in the presence of NaAc is shorter but still 1.5-fold longer than the control (Fig. 3a). This likely results from a counter effect of Na^+ and Ac^-, while Ac^- induced rescues, Na^+ caused catastrophe events (Fig. 2d and f). Consistent with the results that KCl only slightly reduced microtubule polymerization, the microtubule mean length was reduced slightly, while microtubules grown in the presence of 100 mM NaCl were only one-third of the control length (Fig. 3a).

Microtubule nucleation boosted by KAc

Templated nucleation of microtubules, nucleation from seeds, is kinetically unfavorable (43). This is likely due to structural differences between the tapered dynamic microtubule ends and the double-stabilized GMPCPP (a slow hydrolyzable analog of GTP) Taxol seeds, which tend to be blunter. Given that Ac^- boosts spontaneous nucleation (Figs. 1a and 2a), we asked whether Ac^- might promote templated microtubule nucleation. To address this, we measured the efficiency of seeds to nucleate microtubules in the presence of the different ions within 25 min (see Materials and methods). On average 80% of the seeds polymerized microtubules in the control conditions, a ratio unchanged by the addition of either 50 mM KCl or 50 mM NaCl to the assay (Fig. 3b). However, increasing the concentration to 100 mM salt reduced microtubule formation by 1.25-fold (KCl) and 2.3-fold (NaCl). Thus, NaCl has the dual effect of enhancing polymerization speed while hindering new microtubule growth from seeds. This is further supported by the absence of microtubule polymerization beyond 100 mM NaCl (Fig. 2a).

In contrast to NaCl, the addition of 50 mM KAc to the reaction boosted templated microtubule nucleation to 100%. With 100 mM Kac, we observed not only microtubule polymerization from each single seed but also spontaneous nucleation in the bulk—a phenomenon that we observed only above 15 μM tubulin in the absence of KAc (Fig. 2a). At 150 mM KAc and 7 μM tubulin, spontaneous nucleation was so pronounced that analysis of dynamic parameters became unfeasible due to the dense network, a condition resembling what we achieved at 20 μM tubulin in the absence of KAc (Fig. 2a). The efficiency of the microtubule formation in the presence of 50 mM NaAc was reduced compared with the control condition but increased with increasing NaAc concentration (Figs. 1a and 3b). This result underscores a potential counteractive interplay between the anion Ac^- and the cation Na^+, where increasing concentrations of Ac^- drive both templated and de novo nucleation even in the presence of Na^+.

Microtubule aging accelerated by sodium

The probability of a microtubule to undergo catastrophe increases with its lifetime (44–47). This aging process is likely due to the growing GTP cap becoming more irregular and tapered over time, leading to a reduction in the GTP density, which triggers catastrophe events (45, 48). To explore how ions influence this aging process, we studied their impact on the growth span of microtubules before the first catastrophe event occurred. The presence of KCl did not impact microtubule growth span, while the presence of 100 mM NaCl reduced the growth span by 6-fold compared with the control (Fig. 3c). Despite the general destabilizing effect of ions on microtubules (49–51), KAc nearly doubled the growth span relative to the control. Our results show that NaCl and KAc differentially affect aging of microtubules. In a scenario where aging depends on the structure of the GTP cap, NaCl would extend the tapper length of the GTP cap, while KAc would lead to a blunter end.

Impact of nucleotide on salt-driven disassembly

To address the impact of salts on microtubule stability, we monitored depolymerization of GMPCPP-stabilized microtubules in the absence of free tubulin (Fig. 3d). These GMPCPP microtubules, which have more uniformly blunt ends compared with the variably aged ends of dynamic GTP microtubules (44, 52), provided: (i) a more consistent environment to study how salts affect dimer dissociation, (ii) a slower depolymerization that allows us to capture fast processes that might go unnoticed during rapid depolymerization of GDP microtubules, and (iii) a different nucleotide (Fig. 3d). The salt $CaCl_2$ rapidly depolymerizes GMPCPP microtubules (53). We confirmed this and observed that 2 mM $CaCl_2$ depolymerized all GMPCPP microtubules within 100 s (Fig. 3d). The effects of the major salts used in this study were less pronounced; notably, 100 mM NaCl was the most effective destabilizer, reducing the microtubule mass by 50% within 2,000 s, consistent with the effect of NaCl on the mean microtubule length (Fig. 3a). The presence of 100 mM KCl slightly enhanced GMPCPP-microtubule disassembly. Surprisingly, 100 mM NaAc maintained the microtubule polymer compared with the control, indicating a stabilizing effect by either acting on the tip structure or on GMPCPP hydrolysis.

Ions effect on tubulin–tubulin interaction in a GDP lattice

The various salts distinctly influenced microtubule dynamics. To distinguish whether these effects came from alterations in the GTP-hydrolysis rate or from changes in tubulin–tubulin interactions, we study the impact of salts on a homogenous GDP lattice, specifically the microtubule shaft (Fig. 4a). We end-stabilized GDP microtubules and performed a damage assay in the absence of free tubulin to monitor the microtubule breaking process for over 35 min (Fig. 4b). KCl, which did not affect microtubule tip dynamics, also showed no significant differences in shaft dynamics compared with the control (Fig. 4c). However, with NaCl, 100% of the microtubule broke, compared with 85% in the control condition (Fig. 4c). Conversely, only 30% of microtubules broke when incubated with KAc. Microtubule breaking is reduced to 70% when incubated with NaAc, reinforcing our observation of the contrasting effect between Ac^- and Na^+. This result shows that NaCl, NaAc, and KAc act on tubulin–tubulin interactions and not on the hydrolysis rate. Like the case at the tip, at the microtubule shaft, Na^+ destabilizes the interactions and Ac^- has a stabilizing effect.

The damage process of microtubule is affected by ions

To delve deeper into the breaking dynamics of microtubules in the presence of different salts, we measured the time it took for a microtubule to break (Fig. 4d). Since microtubules rapidly depolymerize postbreakage (45, 54), we defined the breakage event as the moment when the microtubule began to depolymerize (yellow arrowhead Fig. 4b). These results showed that microtubule break much faster in the presence of NaCl compared with the control, reducing the microtubule's lifetime by 37% (Fig. 4d). Surprisingly, while microtubules in the presence of KAc and NaAc had lifetimes comparable with the control, those incubated with KCl had a 1.3-fold increase in lifetime before breakage occurred, indicating a protective effect of KCl against breakage. Consistent with this, we observe a delay in the damage formation in the presence of KCl (Fig. 4e).

Although NaCl induced faster damage formation compared with the control (Fig. 4e), the duration from when the damage event occurred to when the microtubule ultimately broke was the same in both conditions (Fig. 4f). This was also the case for KCl and KAc, although the values are slightly higher. Only microtubules incubated with 100 mM NaAc were significantly more stable in this transition state, damage initiation to breakage,

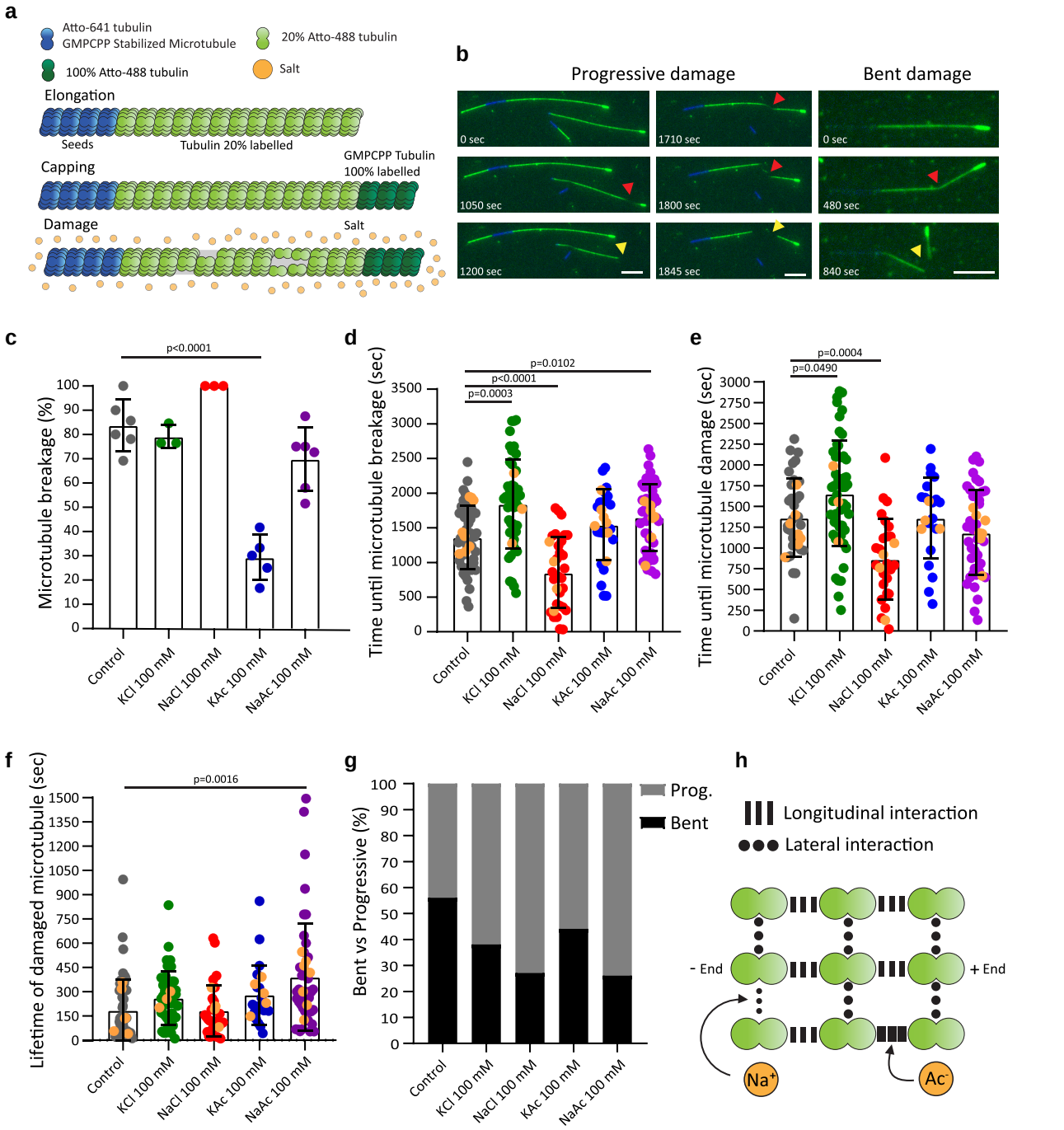

Fig. 4. Ion effect on microtubule damage. a) Scheme of the damage assay. Salts were added during the damage step. b) Representative TIRF images of microtubules showing progressive and bent damage over time. The first two columns show the same microtubules. Red arrowhead: damage site; yellow arrowhead: breakage of microtubule followed by depolymerization. Scale bar: 5 μm. c) Mean microtubule breaking (number of broken microtubules/the total number of microtubules). d) Mean time until microtubule breakage (with the indicated salt), from the beginning of the assay until microtubule started to depolymerize, as indicated by the yellow arrowhead in (b). e) Mean time until microtubule damage (with the indicated salt), from the beginning of the assay until the first sign of damage. f) Mean lifetime of damaged microtubules (seconds until microtubule depolymerized—seconds of first damage sign), with the indicated salt. d–f) Experimental mean with SD, n = at least three independent experiments, individual values, and experimental mean values (orange dots). Statistics: one-way ANOVA. g) Percentage between the two different damaged types with indicated 100 mM salt or 0 mM (control). h) Scheme of the ionic effects of Na^+ and Ac^- on the longitudinal and the lateral interactions of tubulin within the microtubule structure.

increasing this transition time by up to 2.1-fold (Fig. 4f). These results imply that although NaCl can initiate dimer dissociation from the shaft (Fig. 4c–g), it does not influence the subsequent lateral extension of damage leading to breakage. This points to a unique impact of salts on the longitudinal vs. lateral tubulin interactions within the lattice.

Impact of salts on lateral and longitudinal tubulin–tubulin interactions

To study the potential impact of salt on these tubulin–tubulin interactions, we categorized the observed damages into two types: (i) progressive damage, marked by a longitudinally extending decrease in fluorescent intensity that results in mechanically instable

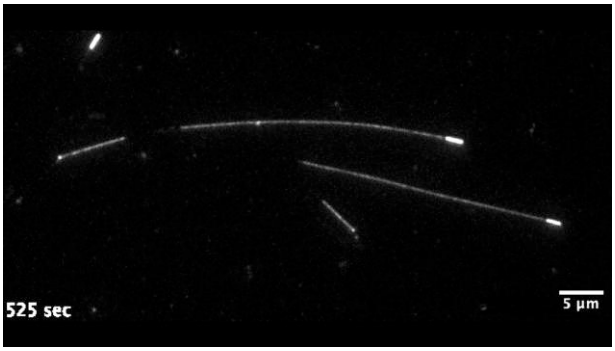

Movie. Microtubule showing progressive damage.

stretches that were wavering in and out of the field of view (see Movie, Fig. 4b) and (ii) bent damage, characterized by an over 170° angle bending of the microtubule before the breakage, likely due to more lateral spreading of the damage (Fig. 4b). The time required of these two damage types to initiate was comparable (red arrowhead in Figs. 4b and S2a). In the control condition, both damage types occurred with equal probability (Fig. 4g). However, the addition of salts shifted the likelihood toward progressive damage, with a maximum for NaCl and NaAc that had three-fourth of the damage in the progressive type (Fig. 4g). These results support the idea that salts weaken lateral interactions, allowing protofilaments to peel out of the lattice (Figs. 4h and S2b, see also Discussion).

Incorporation of GTP tubulin into the microtubule shaft is altered by the ionic composition

We next studied whether the dynamics at the growing tip are differentially affected by salts compared with the more defined and rigid environment at the microtubule shaft. To do so, we performed our breakage assay in the presence of free GTP tubulin, enabling the repair of damage sites (incorporation assay) and studied the impact of 100 mM salt on microtubule shaft dynamics (Fig. 5a and b). Consistent with our data from the breakage assay, in the presence of NaCl, the number of incorporation events per micrometer increased by 2.5-fold compared with the control (Fig. 5c). Similarly, in the presence of NaAc, the incorporation density increased by 1.8-fold. No significant changes were observed with either KAc or KCl. The presence of Na^+ salts uniquely led to an increase in the number of repaired damages.

Furthermore, all salts tested increased the mean length of the incorporation sites, reaching a 2-fold increase with KAc compared with the control (Fig. 5d). This supports our observation that salts prompt progressive damage. These results indicate distinct effects of salts on both the dissociation and incorporation of tubulin dimers at damage sites. While KAc had no effect on the number of damage events, it led to the longest incorporation stretches, suggesting either increased longitudinal dissociation of dimers once damage occurs or higher repair efficiency.

The total fraction of exchanged tubulin along the shaft was highest in the presence of NaCl, followed by NaAc, at 4- and

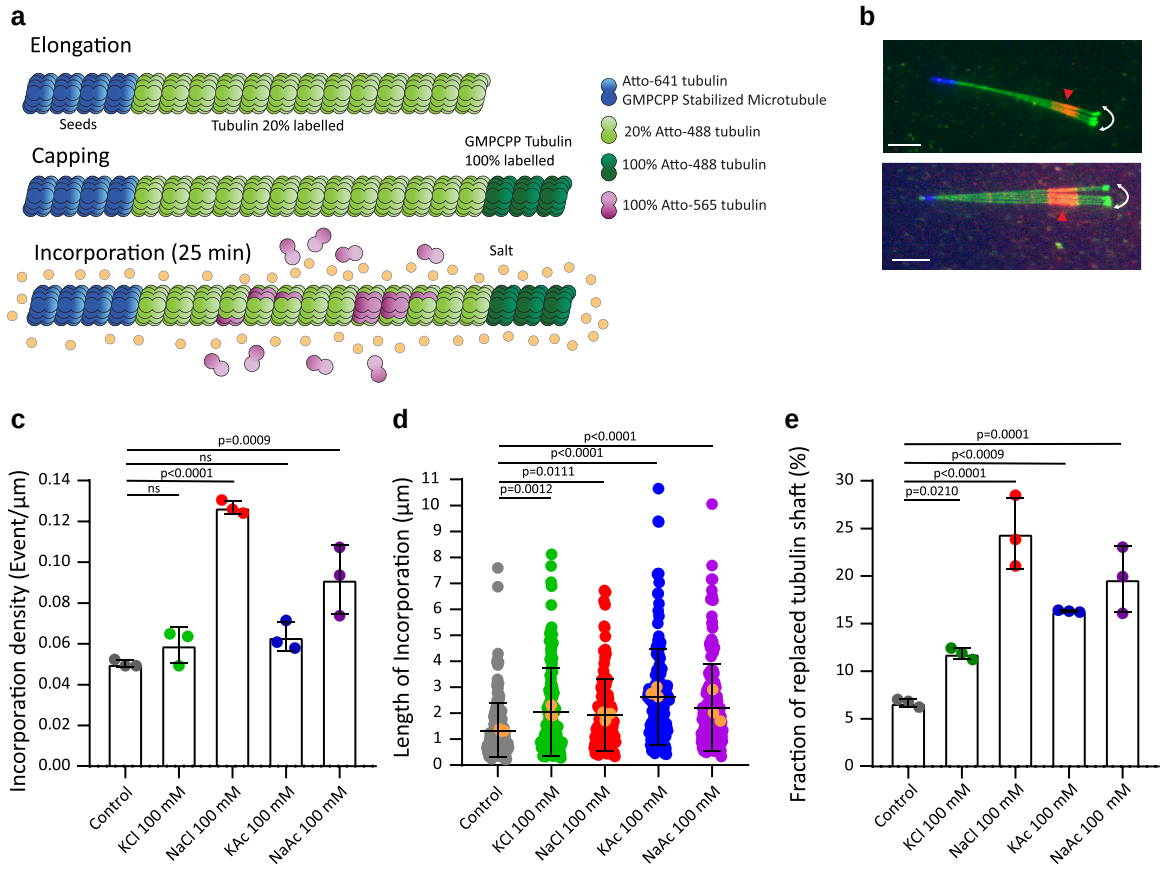

Fig. 5. Ion effect on microtubule shaft dynamic. a) Scheme of the incorporation assay. Salts were added during the incorporation step for 25 min. b) Representative time projection (max intensity) of repaired microtubules after the incorporation assay. Scale bar: 5 µm. c) Mean incorporation density (event/µm) with the indicated 100 mM salt or 0 mM (control). Experimental mean with SD, $n = 3$ independent experiments. d) Mean length of incorporation sites with indicated salt. Experimental mean with SD, $n = 3$ independent experiments, individual values, and experimental mean values (orange dots). e) Mean fraction of replaced tubulin shaft (total length of incorporation sites/total microtubule length) with indicated salt. Experimental mean with SD, $n = 3$ independent experiments. c–e) Statistics: one-way ANOVA.

3-fold, respectively, compared with the control (Fig. 5e). Thus, the number of events was more influential than the net repair efficiency, with KAc showing a 2.6-fold increase. Taken together, the microtubule incorporation assay revealed that the dynamics at both the growing microtubule tip and the shaft are regulated by the ionic composition surrounding the microtubule.

Discussion

Our results show that monovalent ions significantly affect microtubule dynamics. Using dynamic in vitro assays combined with TIRF microscopy, we could precisely characterize the specific effect of these ions on microtubule dynamics and found a strong effect of Na^+ and Ac^- on microtubule stability. Interestingly, some dynamic parameters, such as rescue frequency, polymerization, and depolymerization speed, seemed to have already reached maximum changes at 50 mM salt, while catastrophe frequency continued to increase with higher salt concentrations. This indicates that different dynamic parameters may be governed by distinct electrostatic interactions or ionic interactions. Notably, 100 mM NaCl affects microtubule dynamics similarly to proteins that interact with microtubule ends, such as end-binding proteins, thereby modulating microtubule dynamics (55–59).

Throughout this study, Na^+ had a pronounced destabilizing effect on the microtubule structure. Unlike a previous study using a combination of Taxol and NaCl (39), our data show that net microtubule mass formation is not favored in the presence of Na^+. This cation increases the catastrophe frequency, leading to shorter microtubules with reduced lifetimes (Figs. 2d and 3a–c). Similar to Ca^{2+}, Na^+ induces microtubule depolymerization (37, 38). However, the required concentration of Ca^{2+} to efficiently disassemble the microtubule structure is about 1,000 times lower than that required for Na^+ (0.1 and 100 mM, respectively) (60). Ca^{2+} is proposed to induce depolymerization by interacting with the C-terminal tail of tubulin (61, 62), while simulations predicted that Na^+ is present both at the surface and inside the microtubule lumen (63). Whether Na^+ binds to specific regions associated with tubulin–tubulin interaction remains elusive.

Our damage and incorporation assays (Figs. 4 and 5) suggest that Na^+ weaken lateral interactions between tubulin heterodimers (Fig. 4h). This weakening likely accounts for the higher catastrophe frequency (Fig. 2d), as microtubule associated proteins that disrupt lateral interactions also cause microtubule depolymerization (46). Moreover, weakened lateral interactions are a common presetting to microtubule catastrophe, as GTP hydrolysis weakens lateral interactions (64). These weaker tubulin interactions could furthermore explain the increase in microtubule damage sites, leading to either more repair or breakage events (Figs. 4 and 5). Additionally, weakened lateral interactions could lead to protofilament peeling, where protofilaments progressively peel out from the microtubule shaft. Our results showing expanded progressive damage in the presence of Na^+ would support such a scenario (Fig. 4g). Furthermore, protofilament peeling could explain the general observation that damage sites are often in the range of micrometers (Fig. 5d) (17, 19, 22, 65).

In contrast to Na^+, Ac^- promotes microtubule formation and stability. The presence of Ac^- strongly increased rescue frequency (Fig. 2f), leading to longer microtubules with extended lifetimes (Fig. 3a and c). This increase in rescue frequency was not linked to an increase in incorporation sites along the microtubule lattice (Fig. 5c). The higher incorporation efficiency of KAc and NaAc might be linked to their ability to trigger the highest rescue frequencies. However, NaCl, which had the highest number of incorporation sites, did not influence the rescue frequency. Thus, the increase in rescue frequency observed with KAc and NaAc likely stems from effects at the dynamic end of the microtubule, rather than from changes in shaft dynamics.

We hypothesize that Ac^- stabilizes longitudinal interactions between tubulin heterodimers once integrated into the microtubule structure (Fig. 4h). This enhancement of interactions is further supported by the increase in nucleation efficiency (Fig. 1a and b), as longitudinal interactions are crucial for the nucleation process (66, 67). Furthermore, the damage assay revealed a protective role of Ac^- against microtubule breakage during the assay (Fig. 4c), while Ac^- led to the longest incorporation stretches (Fig. 5d). In summary, in the presence of Ac^-, microtubules break less but exhibit the highest incorporation length compared with other conditions (Fig. 5c–e), indicating that Ac^- enhances repair efficiency.

Our data suggest that Ac^- counteracts the effects of Na^+, while the Cl^- anion might synergize with Na^+, leading to increased polymerization and depolymerization speeds in the presence of NaCl. The observed increase in repair sites with NaAc, alongside reduced breakage, reflects the opposing actions of Na^+ in inducing damage and Ac^- in stabilizing damaged microtubules, preventing breakage. Furthermore, the interplay between the two ions increased microtubule length, increased the rescue frequency, and enhanced net microtubule formation. This is especially pronounced at higher concentrations where 150 mM KAc nucleated microtubules, NaAc mildly nucleated microtubules, and no microtubules were observed for NaCl. However, in terms of microtubule polymerization speed and catastrophe frequency, the effects of Na^+ predominated over those of Ac^-. Further studies into the molecular mechanisms by which salts, particularly Na^+ and Ac^-, affect distinct microtubule dynamic parameters at the protein interaction level would be insightful.

In conclusion, the identity of the ion plays a more predominant role in the modulation of microtubule dynamics than its associated charge. While Na^+ destabilizes the microtubule structure and Ac^- boosts microtubule formation, K^+ and Cl^- did not show any drastic effect on microtubule dynamics. Therefore, the ionic environment in which microtubules grow must be considered according to the specific research question being addressed.

Materials and methods

Tubulin purification from bovine brain and tubulin labeling

Tubulin was purified from fresh bovine brain by two cycles of polymerization and depolymerization, as previously described (68). A first polymerization–depolymerization cycle was performed in high-molarity 1,4-Piperazinediethanesulfonic acid (PIPES) buffer (1 M PIPES-KOH at pH 6.9, 10 mM $MgCl_2$, 20 mM EGTA, 1.5 mM ATP, and 0.5 mM GTP) supplemented with 1:1 glycerol and depolymerization buffer (50 mM MES-HCl at pH 6.6 and 1 mM $CaCl_2$), respectively. A second polymerization–depolymerization cycle was then performed: polymerization in high-molarity PIPES buffer and depolymerization in 0.25XBRB80 complete after 15 min with 5XBRB80 to reach 1XBRB80 (80 mM PIPES at pH 6.8, 1 mM $MgCl_2$, and 1 mM EGTA), respectively.

Labeled tubulin with ATTO-488, ATTO-565, or ATTO-647 (ATTO-TEC GmbH) and biotinylated tubulin were prepared, as previously described (69), with slight modifications. Tubulin was polymerized in glycerol PB solution (80 mM PIPES-KOH at pH 6.8, 5 mM $MgCl_2$, 1 mM EGTA, 1 mM GTP, and 33% [v/v] glycerol) for

30 min at 37 °C and layered onto cushions of 0.1 M NaHEPES at pH 8.6, 1 mM $MgCl_2$, 1 mM EGTA, and 60% (v/v) glycerol followed by centrifugation. The pellet was resuspended in resuspension buffer (0.1 M NaHEPES at pH 8.6, 1 mM $MgCl_2$, 1 mM EGTA, 40% [v/v] glycerol) and incubated 10 min at 37 °C with 1/10 volume of 100 mM ATTO-488, ATTO-565, or ATTO-647 NHS-fluorochrome or incubated 20 min at 37 °C with 2 mM biotin reagent. Labeled tubulin was sedimented onto cushions of BRB80 supplemented with 60% glycerol and resuspended in BRB80. A second polymerization–depolymerization cycle was performed before use. The labeling ratio was 11% for ATTO-488 and 13% for ATTO-565.

Microtubule seeds preparation

Microtubule seeds were prepared by mixing 20% ATTO-647-labeled tubulin and 80% biotinylated tubulin to have a final concentration of 10 μM in BRB80 with 0.5 mM GMPCPP. The solution was incubated at 37 °C for 45 min. One micromolar Paclitaxel was added to the solution and incubated at 37 °C for 30 min. The solution was then centrifuged at 50,000 rpm at 25 °C for 15 min. The pellet was resuspended with BRB80 supplemented with 1 μM Paclitaxel and 0.5 mM GMPCPP. Seeds were aliquoted and stored in liquid nitrogen.

Imaging

Microscopy images were taken with an Axio Observer Inverted TIRF microscope (Zeiss, 3i) and a Prime BSI (Photometrics). A 100× objective (Zeiss, Plan-Apochromat 100×/1.46 oil DIC (UV) VIS-IR) was used. SlideBook 6 X64 software was used to record time-lapse imaging. Microscope stage conditions were controlled with the Chamlide Live Cell Instrument incubator (37 °C).

Flow chamber

Slides and coverslips were cleaned by two successive incubations and sonication: sonicated for 40 min in 1 M NaOH, rinsed in bidistilled water, sonicated in ethanol (96%) for 30 min and rinsed in bidistilled water. Stocks of tri-ethoxy-silane-PEG-biotin and tri-ethoxy-silane-PEG were prepared at 1 mg/mL in 96% ethanol and 0.02% HCl. Slides and coverslips were dried with an air gun, placed into a Plasma cleaner (Electronic Diener, Plasma surface technology) for plasma treatment, followed by 2 days incubation with tri-ethoxy-silane-PEG (Creative PEGWorks) or a mixture of tri-ethoxy-silane-PEG-biotin and tri-ethoxy-silane-PEG with the ratio of 1:5 with gentle agitation at room temperature. Slides and coverslips were then washed in ethanol (96%) and bidistilled water, dried with air gun and stored at 4 °C. Flow chamber was assembled by fixing with double tap a tri-ethoxy-silane-PEG-treated slide with a mixture of tri-ethoxy-silane-PEG-biotin and tri-ethoxy-silane-PEG-treated coverslip with the ratio of 1:5. The volume of the chamber is around 10 μL.

Microtubule dynamic assay

The in vitro chamber was prepared by injecting successively 95 μL of 50 μg/mL neutravidin (5 min incubation), one-time 95 μL BRB80 wash, 95 μL microtubule seeds diluted in BRB80 (20% ATTO-647-labeled tubulin and 80% biotinylated tubulin) and washed three-times with 95 μL BRB80 to remove unattached seeds. A polymerization solution containing: 7 μM tubulin (20% ATTO-488-labeled tubulin, 80% unlabeled), an antibleaching buffer (1 mM GTP, 10 mM DTT, 0.3 mg/mL glucose, 0.1 mg/mL glucose oxidase, 0.02 mg/mL catalase, and 0.125% methyl cellulose [1,500 cP, Sigma]) and 0 mM (control) or 50 or 100 mM salt or 150 mM (KCl, NaCl, KAc, NaAc freshly prepared with bidistillated water from 1 M stock solutions) was prepared. The volume was completed to 30 μL with 1× BRB80. The polymerization solution was injected in the chamber, and the chamber was sealed for microscopy analysis. Microtubule polymerization was recorded over 300 frames at the interval of 5 s. High-speed measurement was performed at 1 s intervals (Fig. S1f and g). Kymographs were generated and analyzed using an ImageJ macro. Polymerization and depolymerization speeds were measured with the slope in the kymographs (Fig. S1a). Each analysis point in the panel, Fig. S1b and d, corresponds to one slope in a kymograph (Fig. S1a). Catastrophe frequency was calculated with the number of catastrophes spent during growth (frequency = number of catastrophe event/time spent in growth). Rescue frequency was calculated as follows: frequency = number of rescue event/time spent in depolymerization. Catastrophe and rescue events are, respectively, highlighted by a red star and a green rectangle in Fig. S1a. Microtubule mean length was measured from the onset of microtubule growth until the catastrophe event that precedes its full depolymerization. In the case where a microtubule undergoes several catastrophe and rescue events before its full depolymerization, the measured mean length is the average of the different maximal lengths that reach the microtubule before each catastrophe event. In the case where a microtubule does not undergo catastrophe within the acquisition time, the measured length reflects the maximum length during the acquisition. The mean ratio of templated microtubule nucleation was calculated by dividing the number of seeds with nucleated microtubule over the acquisition/total amount of seeds in the field of view. The microtubule lifetime is the time spent during the microtubule growth phase until the first catastrophe event. Graphs were created with GraphPad Prism8. One-way ANOVA was performed for statistics.

Incorporation assay

Incorporation assay was adapted from the protocol published in Ref. (70). In vitro chamber was prepared by injecting successively 95 μL of 50 μg/mL neutravidin (5 min incubation), one-time 95 μL BRB80 wash, 95 μL microtubule seeds diluted in BRB80 (20% ATTO-647-labeled tubulin and 80% biotinylated tubulin) and washed three-times with 95 μL BRB80 to remove unattached seeds. A polymerization solution containing: 10 μM tubulin (20% ATTO-488-labeled tubulin, 80% unlabeled), BRB80, and an antibleaching buffer (1 mM GTP, 10 mM DTT, 0.3 mg/mL glucose, 0.1 mg/mL glucose oxidase, 0.02 mg/mL catalase, 0.125% methyl cellulose [1,500 cP, Sigma]) was perfused in the chamber. The chamber was incubated for 15 min at 37 °C for microtubule polymerization from the seeds. A prewarmed capping solution of 6 μM tubulin (100% ATTO-488-labeled tubulin) in BRB80 supplemented with 0.5 mM GMPCPP was perfused in the chamber to exchange the polymerization buffer and then incubated for 15 min at 37 °C. The chamber was washed twice with 95 μL prewarmed BRB80 to remove unattached GMPCPP microtubules. An incorporation buffer containing: 10 μM tubulin (100% ATTO-565-labeled tubulin) in BRB80 supplemented with 0 mM (control) or 100 mM salt (KCl, NaCl, KAc, NaAc freshly prepared with bidistillated water from 1 M stock solutions) was injected in the chamber and incubated at 37 °C for 25 min. The chamber was washed with prewarmed 95 μL BRB80 and an imaging solution of 6 μM tubulin (unlabeled) with BRB80 supplemented with antibleaching buffer was injected in the chamber. The chamber was sealed for microscopy analysis. Each position was recorded over 10 frames. Only fluctuating microtubules (Fig. 5b) were considered in the analysis to ensure that the

measured incorporation signal was not from an aggregate stacked on the surface. The mean incorporation density was calculated with the number of incorporation sites/the total microtubule length. The mean fraction of replaced tubulin in the shaft was calculated with the total length of incorporation/the total microtubule length. Measurements were done with Fiji. Graphs and statistical analysis (one-way ANOVA) were performed with GraphPad Prism8.

Damage assay

Damage assay follows the same steps as the incorporation assay (explained above) until the capping solution incubation. The chamber was washed twice with 95 μL prewarmed BRB80 to remove unattached microtubules. An imaging solution containing: antibleaching buffer, BRB80 0 mM (control) or 100 mM salt (KCl, NaCl, KAc, and NaAc were freshly prepared with bidistillated water from 1 M stock solutions) and complete to 30 μL with BRB80 was perfused in the chamber. The chamber was sealed for microscopy imaging. Each position was recorded over 200 frames with an interval of 10 s. Only fluctuating microtubules were considered in the analysis to prevent any hypothetical glass-stabilizing interaction with microtubules. The mean microtubule breaking ratio was calculated with the total number of broken microtubule/the total number of microtubules. The time required for breakage was measured from the beginning of the acquisition until the microtubule breakage. The time required to damage a microtubule was measured from the beginning of the acquisition until the first appearance of the damage sign. The mean lifetime of damaged microtubules was measured by subtracting the time required to break a microtubule from the time required to damage a microtubule. All the measurements were performed with Fiji. The graphs and the statistical analysis (one-way ANOVA) were performed with GraphPad Prism8.

Turbidity assay

Two microliters of 15 μM tubulin (unlabeled) were prepared in a BRB80 buffer supplemented with 1 mM GTP, 20% glycerol (v/v), and 0 mM (control) or 50 mM or 100 mM salt (KCl, NaCl, KAc, and NaAc were freshly prepared with bidistillated water from 1 M stock solutions). Solutions were transferred into a 96-well plate for turbidity analysis at 37 °C. Absorbance was measured at 350 nm every 30 s over 3,500 s with a Spectra MAX instrument. A control well (only BRB80) was included in the experiment to subtract the background. Data were extracted and processed with Microsoft Excel. A nonlinear regression (logistic fit; equation: $Y = YM \times Y0/(YM - Y0) \times \exp(-k \times x) + Y0$, where Y0 is the starting population [here $Y0 = 0$], YM is the maximal value [plateau], and k is the rate constant of the curve) was applied on the graph to calculate the lag time, the plateau, and the slope of the curve (Fig. 1b), with GraphPad Prism 8. One-way ANOVA was used to calculate statistics.

Microtubule polymerization assay

A 10-μM tubulin (unlabeled) was polymerized in a BRB80 buffer supplemented with 1 mM GTP, 20% glycerol (v/v), 0 mM (control), or 200 mM salt (NaCl or KAc were freshly prepared with bidistillated water from 1 M stock solutions) and incubated for 30 min at 37 °C. The solution was centrifuged at 50,000 rpm at 37 °C for 20 min. The supernatant was harvested, and the pellet was resuspended in BRB80 buffer (similar volume as the starting volume). Samples were loaded in a sodium dodecyl sulfate–polyacrylamide gel electrophoresis (SDS–PAGE) gel followed by a Coomassie staining. Band intensities were measured on ImageJ and then plotted and analyzed with GraphPad Prism 8. Two-way ANOVA was used to calculate statistics.

GMPCPP microtubule survival assay

A 10-μM tubulin (20% labeled ATTO-488) was polymerized in a BRB80 buffer supplemented with 0.5 mM GMPCPP for 30 min at 37 °C. GMPCPP microtubules were then mixed with antibleaching buffer (without GTP) and with 0 (Ctrl) or 2 mM $CaCl_2$ (freshly prepared with bidistillated water from a 0.5-M stock solution) or 100 mM of salt (KCl, NaCl, KAc, and NaAc were freshly prepared with bidistillated water from 1 M stock solutions). Please note that EGTA was present in the BRB80; in the observed result at 2 mM $CaCl_2$, it needs to be considered that some of the Ca^{2+} were chelated by EGTA. Two hundred frames were recorded with an interval of 10 s. An arbitrary region with fixed size was randomly selected to measure the intensity over time for all experiments. Background intensity (selected region where no GMPCPP microtubules were present) was subtracted from the measured integrated fluorescent intensity. The resulting value was normalized to 1, and the changes in fluorescent intensity were plotted over time. Measurements were performed with ImageJ, and the graph plotted and statistical analysis (one-way ANOVA) were performed with GraphPad Prism8. Linear regressions were applied for each condition ($Y = \text{slope} \times x$, $Y0 = 1$ as a restriction).

Acknowledgments

The authors thank M. Andreu-Carbó and Pei-Tzu Yang for carefully reading the manuscript and ChatGPT for spelling and punctuation correction.

Supplementary Material

Supplementary material is available at *PNAS Nexus* online.

Funding

S.F. and C.A. have been supported by the DIP of the Canton of Geneva and the SNSF (TMSGI3_211433).

Author Contributions

S.F. and C.A. conceptualized the project. S.F. performed and analyzed the in vitro dynamic assays, sedimentation experiments, incorporation, and breakage assay under the supervision of C.A. S.F. and C.A. wrote the manuscript.

Preprints

This manuscript was posted on a preprint: https://doi.org/10.1101/2024.06.26.600768.

Data Availability

All data associated with this study are presented in the article.

References

1 Desai A, Mitchison TJ. 1997. Microtubule polymerization dynamics. *Annu Rev Cell Dev Biol*. 13:83–117.
2 Schulze E, Kirschner M. 1986. Microtubule dynamics in interphase cells. *J Cell Biol*. 102:1020–1031.

3 Behnke O. 1964. A preliminary report on "microtubules" in undifferentiated and differentiated vertebrate cells. *J Ultrastruct Res*. 11:139–146.
4 Croom HB, Correia JJ, Williams RC. 1986. The effects of elevated pH and high salt concentrations on tubulin. *Arch Biochem Biophys*. 249:397–406.
5 Haga T, Abe T, Kurokawa M. 1974. Polymerization and depolymerization of microtubules in vitro as studied by flow birefringence. *FEBS Lett*. 39:291–295.
6 Kuriyama R, Sakai H. 1974. Viscometric demonstration of tubulin polymerization. *J Biochem*. 75:463–471.
7 Lee YC, Samson FE, Houston LL, Himes RH. 1974. The in vitro polymerization of tubulin from beef brain. *J Neurobiol*. 5:317–330.
8 Olmsted JB, Borisy GG. 1975. Ionic and nucleotide requirements for microtubule polymerization in vitro. *Biochemistry*. 14:2996–3005.
9 Suzaki T, Sakai H, Endo S, Kimura I, Shigenaka Y. 1978. Effects of various anions, glutamate and GTP on microtubule assembly in vitro. *J Biochem*. 84:75–81.
10 Weisenberg RC. 1972. Microtubule formation in vitro in solutions containing low calcium concentrations. *Science*. 177:1104–1105.
11 Valiron O, Caudron N, Job D. 2001. Microtubule dynamics. *Cell Mol Life Sci*. 58:2069–2084.
12 Hyman AA, Salser S, Drechsel DN, Unwin N, Mitchison TJ. 1992. Role of GTP hydrolysis in microtubule dynamics: information from a slowly hydrolyzable analogue, GMPCPP. *Mol Biol Cell*. 3: 1155–1167.
13 Nogales E, Downing KH, Amos LA, Löwe J. 1998. Tubulin and FtsZ form a distinct family of GTPases. *Nat Struct Biol*. 5:451–458.
14 Bowne-Anderson H, Hibbel A, Howard J. 2015. Regulation of microtubule growth and catastrophe: unifying theory and experiment. *Trends Cell Biol*. 25:769–779.
15 Farmer VJ, Zanic M. 2023. Beyond the GTP-cap: elucidating the molecular mechanisms of microtubule catastrophe. *Bioessays*. 45:e2200081.
16 Mitchison T, Kirschner M. 1984. Dynamic instability of microtubule growth. *Nature*. 312:237–242.
17 Andreu-Carbó M, Fernandes S, Velluz M-C, Kruse K, Aumeier C. 2022b. Motor usage imprints microtubule stability along the shaft. *Dev Cell*. 57:5–18.e8.
18 Dimitrov A, *et al*. 2008. Detection of GTP-tubulin conformation in vivo reveals a role for GTP remnants in microtubule rescues. *Science*. 322:1353–1356.
19 Schaedel L, *et al*. 2019. Lattice defects induce microtubule self-renewal. *Nat Phys*. 15:830–838.
20 Triclin S, *et al*. 2021. Self-repair protects microtubules from destruction by molecular motors. *Nat Mater*. 20:883–891.
21 Tropini C, Roth EA, Zanic M, Gardner MK, Howard J. 2012. Islands containing slowly hydrolyzable GTP analogs promote microtubule rescues. *PLoS One*. 7:e30103.
22 Aumeier C, *et al*. 2016. Self-repair promotes microtubule rescue. *Nat Cell Biol*. 18:1054–1064.
23 Sheinerman FB, Norel R, Honig B. 2000. Electrostatic aspects of protein-protein interactions. *Curr Opin Struct Biol*. 10:153–159.
24 Zhou H-X, Pang X. 2018. Electrostatic interactions in protein structure, folding, binding, and condensation. *Chem Rev*. 118: 1691–1741.
25 Drechsler H, Xu Y, Geyer VF, Zhang Y, Diez S. 2019. Multivalent electrostatic microtubule interactions of synthetic peptides are sufficient to mimic advanced MAP-like behavior. *Mol Biol Cell*. 30:2953–2968.
26 Tuszyński JA, *et al*. 2005. Molecular dynamics simulations of tubulin structure and calculations of electrostatic properties of microtubules. *Math Comput Model*. 41:1055–1070.
27 Cacace MG, Landau EM, Ramsden JJ. 1997. The Hofmeister series: salt and solvent effects on interfacial phenomena. *Q Rev Biophys*. 30:241–277.
28 Gregory KP, *et al*. 2022. Understanding specific ion effects and the Hofmeister series. *Phys Chem Chem Phys*. 24:12682–12718.
29 Kang B, Tang H, Zhao Z, Song S. 2020. Hofmeister series: insights of ion specificity from amphiphilic assembly and interface property. *ACS Omega*. 5:6229–6239.
30 Okur HI, *et al*. 2017. Beyond the Hofmeister series: ion-specific effects on proteins and their biological functions. *J Phys Chem B*. 121:1997–2014.
31 Rosenfeld AC, Zackroff RV, Weisenberg RC. 1976. Magnesium stimulation of calcium binding to tubulin and calcium induced depolymerization of microtubules. *FEBS Lett*. 65: 144–147.
32 Fees CP, Moore JK. 2019. A unified model for microtubule rescue. *Mol Biol Cell*. 30:753–765.
33 Grover S, Hamel E. 1994. The magnesium-GTP interaction in microtubule assembly. *Eur J Biochem*. 222:163–172.
34 Huang AB, Lin CM, Hamel E. 1985. Differential effects of magnesium on tubulin-nucleotide interactions. *Biochim Biophys Acta*. 832:22–32.
35 Martin SR, Butler FM, Clark DC, Zhou JM, Bayley PM. 1987. Magnesium ion effects on microtubule nucleation in vitro. *Biochim Biophys Acta*. 914:96–100.
36 O'Brien ET, Salmon ED, Walker RA, Erickson HP. 1990. Effects of magnesium on the dynamic instability of individual microtubules. *Biochemistry*. 29:6648–6656.
37 O'Brien ET, Salmon ED, Erickson HP. 1997. How calcium causes microtubule depolymerization. *Cell Motil Cytoskeleton*. 36: 125–135.
38 Weisenberg RC, Deery WJ. 1981. The mechanism of calcium-induced microtubule disassembly. *Biochem Biophys Res Commun*. 102:924–931.
39 Wolff J, Sackett DL, Knipling L. 1996. Cation selective promotion of tubulin polymerization by alkali metal chlorides. *Protein Sci*. 5: 2020–2028.
40 Luchniak A, *et al*. 2023. Dynamic microtubules slow down during their shrinkage phase. *Biophys J*. 122:616–623.
41 Gardner MK, Zanic M, Howard J. 2013. Microtubule catastrophe and rescue. *Curr Opin Cell Biol*. 25:14–22.
42 Schaer J, Andreu-Carbó M, Kruse K, Aumeier C. 2023. The effect of motor-induced shaft dynamics on microtubule stability and length. *Biophys J*. 122:346–359.
43 Wieczorek M, Bechstedt S, Chaaban S, Brouhard GJ. 2015. Microtubule-associated proteins control the kinetics of microtubule nucleation. *Nat Cell Biol*. 17:907–916.
44 Coombes CE, Yamamoto A, Kenzie MR, Odde DJ, Gardner MK. 2013. Evolving tip structures can explain age-dependent microtubule catastrophe. *Curr Biol*. 23:1342–1348.
45 Duellberg C, Cade NI, Surrey T. 2016. Microtubule aging probed by microfluidics-assisted tubulin washout. *Mol Biol Cell*. 27: 3563–3573.
46 Gardner MK, Zanic M, Gell C, Bormuth V, Howard J. 2011. Depolymerizing kinesins Kip3 and MCAK shape cellular microtubule architecture by differential control of catastrophe. *Cell*. 147:1092–1103.
47 Odde DJ, Buettner HM. 1995. Time series characterization of simulated microtubule dynamics in the nerve growth cone. *Ann Biomed Eng*. 23:268–286.
48 Duellberg C, Cade NI, Holmes D, Surrey T. 2016. The size of the EB cap determines instantaneous microtubule stability. *Elife*. 5: e13470.

49 Bonacker D, *et al.* 2005. Genotoxicity of inorganic lead salts and disturbance of microtubule function. *Environ Mol Mutagen*. 45: 346–353.

50 Perchellet EM, Ladesich JB, Collery P, Perchellet JP. 1999. Microtubule-disrupting effects of gallium chloride in vitro. *Anticancer Drugs*. 10:477–488.

51 Shevtsov PN, Shevtsova EF, Burbaeva GS. 2016. Effect of aluminum, iron, and zinc ions on the assembly of microtubules from brain microtubule proteins. *Bull Exp Biol Med*. 161:451–455.

52 Gardner MK, *et al.* 2014. Rapid microtubule self-assembly kinetics. *Cell*. 159:215.

53 Müller-Reichert T, Chrétien D, Severin F, Hyman AA. 1998. Structural changes at microtubule ends accompanying GTP hydrolysis: information from a slowly hydrolyzable analogue of GTP, guanylyl (alpha,beta)methylenediphosphonate. *Proc Natl Acad Sci U S A*. 95:3661–3666.

54 Tang-Schomer MD, Patel AR, Baas PW, Smith DH. 2010. Mechanical breaking of microtubules in axons during dynamic stretch injury underlies delayed elasticity, microtubule disassembly, and axon degeneration. *FASEB J*. 24:1401–1410.

55 Bieling P, *et al.* 2008. CLIP-170 tracks growing microtubule ends by dynamically recognizing composite EB1/tubulin-binding sites. *J Cell Biol*. 183:1223–1233.

56 Komarova YA, Akhmanova AS, Kojima S-I, Galjart N, Borisy GG. 2002. Cytoplasmic linker proteins promote microtubule rescue in vivo. *J Cell Biol*. 159:589–599.

57 Miesch J, Wimbish RT, Velluz M-C, Aumeier C. 2023. Phase separation of +TIP networks regulates microtubule dynamics. *Proc Natl Acad Sci U S A*. 120:e2301457120.

58 Montenegro Gouveia S, *et al.* 2010. In vitro reconstitution of the functional interplay between MCAK and EB3 at microtubule plus ends. *Curr Biol*. 20:1717–1722.

59 Vitre B, *et al.* 2008. EB1 regulates microtubule dynamics and tubulin sheet closure in vitro. *Nat Cell Biol*. 10:415–421.

60 Berkowitz SA, Wolff J. 1981. Intrinsic calcium sensitivity of tubulin polymerization. The contributions of temperature, tubulin concentration, and associated proteins. *J Biol Chem* 256: 11216–11223.

61 Lefèvre J, *et al.* 2011. The C terminus of tubulin, a versatile partner for cationic molecules: binding of Tau, polyamines, and calcium. *J Biol Chem*. 286:3065–3078.

62 Saoudi Y, Paintrand I, Multigner L, Job D. 1995. Stabilization and bundling of subtilisin-treated microtubules induced by microtubule associated proteins. *J Cell Sci*. 108(Pt 1): 357–367.

63 Shen C, Guo W. 2018. Ion permeability of a microtubule in neuron environment. *J Phys Chem Lett*. 9:2009–2014.

64 Akhmanova A, Steinmetz MO. 2015. Control of microtubule organization and dynamics: two ends in the limelight. *Nat Rev Mol Cell Biol*. 16:711–726.

65 Kirschner MW, Williams RC, Weingarten M, Gerhart JC. 1974. Microtubules from mammalian brain: some properties of their depolymerization products and a proposed mechanism of assembly and disassembly. *Proc Natl Acad Sci U S A*. 71: 1159–1163.

66 Caudron N, Arnal I, Buhler E, Job D, Valiron O. 2002. Microtubule nucleation from stable tubulin oligomers. *J Biol Chem*. 277: 50973–50979.

67 Job D, Valiron O, Oakley B. 2003. Microtubule nucleation. *Curr Opin Cell Biol*. 15:111–117.

68 Castoldi M, Popov AV. 2003. Purification of brain tubulin through two cycles of polymerization- depolymerization in a high-molarity buffer. *Protein Expr Purif*. 32:83–88.

69 Hyman AA, *et al.* 1991. Preparation of modified tubulins. *Methods Enzymol*. 196:478–485.

70 Andreu-Carbó M, Fernandes S, Aumeier C. 2022. Two-color in vitro assay to visualize and quantify microtubule shaft dynamics. *STAR Protoc*. 3:101320.